Synthesis, characterization, DNA binding and cleavage, HSA interaction and cytotoxicity of a new copper(II) complex drived from 2-(2'-pyridyl)benzothiazole and glycylglycine

ARTICLE *in* JOURNAL OF PHOTOCHEMISTRY AND PHOTOBIOLOGY A CHEMISTRY · FEBRUARY 2013

Impact Factor: 2.5 · DOI: 10.1016/j.jphotochem.2013.12.002

4 AUTHORS, INCLUDING:

Xue-Yi Le
South China Agricultural University
26 PUBLICATIONS **112** CITATIONS

SEE PROFILE

Journal of Photochemistry and Photobiology A: Chemistry 276 (2014) 83–95

Contents lists available at ScienceDirect

Journal of Photochemistry and Photobiology A: Chemistry

journal homepage: www.elsevier.com/locate/jphotochem

Synthesis, characterization, DNA binding and cleavage, HSA interaction and cytotoxicity of a new copper(II) complex derived from 2-(2′-pyridyl)benzothiazole and glycylglycine

Xia-Bing Fu [a], Gui-Tian Weng [a], Dan-Dan Liu [a], Xue-Yi Le [a,b,*]

[a] Department of Applied Chemistry, South China Agricultural University, Guangzhou 510642, PR China
[b] Institute of Biomaterial, South China Agricultural University, Guangzhou 510642, PR China

ARTICLE INFO

Article history:
Received 18 July 2013
Received in revised form
29 November 2013
Accepted 4 December 2013
Available online 12 December 2013

Keywords:
Copper(II)–dipeptide complex
2-(2′-Pyridyl)benzothiazole
DNA binding
Nuclease activity
HSA interaction
Cytotoxicity

ABSTRACT

A new copper(II) complex, [Cu(glygly)(pbt)(H_2O)]ClO_4 (glygly = glycylglycine anion and pbt = 2-(2′-pyridyl)benzothiazole) was synthesized and characterized by elemental analysis, molar conductivity, mass spectra, IR spectra, UV–vis spectra and thermogravimetric analysis (TGA). Spectroscopic titration, viscosity, and electrophoresis measurements revealed that the complex intercalated to calf thymus (CT)-DNA with moderate binding affinity ($K_b = 5.64 \times 10^4\ M^{-1}$), and cleaved pBR322 DNA at a low concentration of 5 μM in the presence of ascorbic acid, presumably via an oxidative mechanism. Further, the protein-binding ability has been monitored by various spectroscopic techniques (UV–vis, fluorescence and CD) using human serum albumin (HSA) as a model protein. The complex displayed desired affinity to HSA in which hydrophobic interaction played a major role. In addition, the complex was subjected to cytotoxicity tests in vitro using three human cancer cells lines (HepG2, HeLa and A549) and showed prominent and selective cytotoxicity against HepG2 cell lines ($IC_{50} \sim 17.78$ μM).

1. Introduction

Cancer – a growing menace (total global cancer 2008: 12,662,554; 2030: +69%) – is a complex disease of which many people are afraid, and cancer – the big C – will often top the list as the major cause of morbidity and mortality of mankind [1]. Therefore, developing effective antineoplastic drugs for the clinical therapy of tumor is a hard and vital task of the whole body of mankind for a long time. The clinical success of cisplatin for treating most aggressive solid tumors pioneered the extensive researches of platinumbased complexes as the antitumor reagents [2]. However, platinumbased chemotherapeutic agents acting by binding covalently to deoxyribonucleic acid (DNA), are severely affected by their serious side effects, such as general toxicity and acquired drug resistance [3]. Thus, developing effective, target specific, less toxic, and preferably non-covalently binding anticancer drugs for treating chronic diseases is an important challenge for chemists in the area of medicinal chemistry. In this regard, copper complexes is an attractive prospect, with the ability of cleaving DNA by non-covalently binding under physiological conditions, better applications at the cellular level and low toxicity.

Benzothiazole and its derivatives are an important pharmacophores of heterocyclic compounds that exhibit a wide range of pharmacological properties such as herbicidal, pesticidal [4], antimicrobial [5], anticonvulsant [6], cyclooxygenase inhibitors [7], and antitumor in particular [8–11], and thus are widely used in pesticide and medicine field. 2-(2′-pyridyl) benzothiazole (pbt) is one of benzothiazole-based compounds. It coordinates with metal ions mainly by the nitrogen-atoms of pyridyl and thiazole, the generated complexes exhibit various photochemical and photophysical properties besides biological activities. Recent years, many complexes of pbt with transition metal ions (Co^{II} [12], Ni^{II} [12,16], Cu^{II} [12–15], Zn^{II} [13], Fe^{III} [14]), Sn^{II} [17], Pt^{II} [18], Ru [19,20], Tc [21] and Re [21–24] have been reported. It was found that pbt based metal complexes like [Cu(pbt)Br_2] [13] and [Sn(pbt)Cl_2] [17] exhibit remarkable cytotoxic effects against the cancer cell lines, and oxorhenium(V)/oxotechnetium(V) complexes of pbt possess interesting properties for the development of technetium and rhenium radiopharmaceuticals for tumor imaging and/or radiotherapy as well as in vivo diagnosis of Alzheimer's disease [21]. On the other hand, peptides can be used as hormones, enzyme inhibitors, neurotransmitters, and immunomodulators in living systems, and therefore are expected to play an important role in the treatment of many diseases such as cancer, AIDS and Alzheimers [25,26]. Moreover, Cu(II)–peptide complexes may be regarded as models for both

* Corresponding author at: Department of Applied Chemistry, South China Agricultural University, Guangzhou 510642, PR China. Tel.: +86 020 85287010.
E-mail addresses: stacey.quick@yale.edu, xbf200805@163.com, lexyfu@163.com (X.-Y. Le).

1010-6030/$ – see front matter © 2013 Elsevier B.V. All rights reserved.
http://dx.doi.org/10.1016/j.jphotochem.2013.12.002

protein–DNA and antitumor agent–DNA interactions, since peptides are the basic structural units of HSA that recognize a specific base sequence of DNA [27]. Therefore, it was thought worthwhile to assess the pharmacological properties of the pbt based copper(II) complexes with peptides.

Human serum albumin, as the most abundant proteins in the human plasma, acts as transporter and disposer of various endogenous and exogenous substances through circulating in plasma and binding to human serum albumin [28]. Binding of a drug to albumin brings about an increased drug solubility in plasma, decreased toxicity, and protection against oxidation of the bound drug [29]. Furthermore, human serum albumin is known to accumulate in tumors, being taken up by tumor cells at increased levels compared to normal cells, and serves as carrier conjugate of various anticancer drugs viz., chlorambucil, paclitaxel and doxorubicin [30]. Consequently, investigation of the protein binding of drugs in vitro to figure out the pharmacokinetics of drugs and function of human serum albumin in plasma would be pregnant.

In the light of above consideration, in this paper, we have synthesized and characterized a new copper(II) complex derived from 2-(2′-pyridyl)benzothiazole and dipeptide (glycyl glycine anion). The in vitro cytotoxicity was evaluated by MTT assay using three human cancer cells lines (HepG2, HeLa and A549). The DNA-binding and nuclease properties were studied by spectroscopic methods, Viscosity and agarose gel electrophoresis measurements. Additionally, the affinity to human serum albumin in vitro was explored via multispectroscopic techniques (fluorescence, UV–vis and CD). We hope our results may contribute to the rational molecular design of new artificial metallopeptide-nucleases and chemotherapeutic agents with high efficiency and selectivity, and elucidate valuable information to understand their specific delivery at the active site of action, besides providing the pharmacological profile in vitro.

2. Experimental

2.1. Materials and reagents

Caution! Perchlorate salts of metal complexes are potentially explosive and therefore should be prepared in small quantities. NaN_3 serves as explosive in automotive airbags and must not be used with halogenated organic solvents or cosolvent or it may give rise to organic azides [31].

Calf thymus (CT)-DNA was purchased from Sigman (USA), pBR322 DNA from the MBI Fermentas (Lithuania), and human serum albumin (HSA) from the Wako (Japan) and used as received. Human hepatocellular carcinoma cells line (HepG2), human cervical cancer cell line (HeLa) and human pulmonary carcinoma cell line (A549) were obtained from Laboratory Animal Center of Sun yat-sen university. All other chemicals of analytical reagent grade were commercially purchased and used without further purification. Doubly distilled water was used as the solvent throughout the experiments. The stock solution of CT-DNA was prepared in 5 mM Tris–HCl/50 mM NaCl buffer at pH 7.2, which gave a ratio of UV absorbances at 260 nm and 280 nm (A_{260}/A_{280}) of ca. 1.8–1.9, indicating that the DNA was sufficiently free of protein [32], and the concentration was determined by UV absorbance at 260 nm ($\varepsilon = 6600\ M^{-1}\ cm^{-1}$) [33]. The stock solution of HSA was prepared by dissolving the solid HSA in 0.05 M Tris–HCl/0.15 M NaCl buffer at pH 7.4, and the concentration was determined by UV absorbance at 280 nm ($\varepsilon = 35{,}700\ M^{-1}\ cm^{-1}$) [34]. All stock solutions were stored at 4 °C and used within 5 days.

2.2. Physical measurement

Elemental analyses for C, H and N were performed using a Vario EL elemental analyzer (Elementar, Germany). Infrared spectrum (KBr pellet) was recorded on a Nicolet ACATAR 360 FT-IR spectrometer (Nicolet, USA) in the range of 4000–400 cm^{-1}. Molar conductivity was measured on a DDS-11A digital conductometer (LeiCi, China) at room temperature in 1.0×10^{-3} M methanol solution. ESI-MS was processed on a API4000 (AB Sciex, USA). Electronic absorption spectra were carried out on a Pharmacia 2550 UV–vis spectrophotometer (Shimadzu, Japan). Fluorescence measurements were performed on a Hitachi RF-4500 fluorescence spectrophotometer (Hitachi, Japan) equipped with a thermostatic bath, and circular dichroism spectroscopy were recorded on a Chirascan CD spectropolarimeter (Applied Photophysics, UK) at room temperature using a 0.1 cm quartz cuvette. The gel imaging and densitometric analysis were assessed using BIO-RAD Laboratories-Segrate imaging and Gel Documentation Systems.

2.3. Synthesis of ligand 2-(2′-pyridyl)benzothiazole (pbt)

The ligand pbt was prepared by the condensation of 2-aminothiophenol and pyridine-2-carboxaldehyde as reported early [23].

2.4. Synthesis of [Cu(glygly)(pbt)(H_2O)]ClO_4

To a mixture of glygly (0.066 g, 0.5 mmol) and NaOH (0.020 g, 0.5 mmol) in H_2O, an aq. soln. of $Cu(ClO_4)_2{\cdot}6H_2O$ (0.186 g, 0.5 mmol) was added with stirring, followed by the addition of pbt (0.106 g, 0.5 mmol) in ethanol (20 ml). The stirring was continued for ca. 3 h at 60 °C. The resulting solution was filtered off and allowed to evaporate for a few days at room temperature until blue-greenish crystals formed. The resulted product was filtered, dried under vacuum, and further purified by recrystallization from 80% ethanol–water (v/v). Yield: 56% (found: C, 36.72; H, 3.32; N, 10.62; calc. for $C_{16}H_{17}N_4O_8SClCu$: C, 36.65; H, 3.27; N, 10.68%). Molar conductance, Λ_M (1.0×10^{-3} M, MeOH) = 89.5 $\Omega^{-1}\ cm^2\ mol^{-1}$. ESI-MS (*m*/*z*, MeOH): 408.0, $[Cu(glygly)(pbt)]^+$. IR (KBr, cm^{-1}): ν(O—H) 3423, ν_{as}(—NH_2) 3103, ν_s(—NH_2) 2928, ν_{as}(—COO^-) 1625, ν(C=N) 1561, ν(C=C) 1493, ν_s(—COO^-) 1383, $\nu(ClO_4^-)$ 1087, ν(Cu–N) 627, ν(Cu–O) 473. UV–vis (MeOH), λ_{max}/nm ($\varepsilon/M^{-1}\ cm^{-1}$): 225 (13,895), 307 (13,167) and 638 (74.39). TGA: 150–220 °C, loss 3.3% (calc. 3.4%, 18 mass units).

2.5. DNA-binding experiments

2.5.1. Absorption spectra measurements

Absorption titrations were performed for the complex by keeping the concentration of the complex constant (5.0×10^{-5} M), while varying the concentration of CT-DNA via steady addition of CT-DNA (1.0×10^{-3} M). The absorption spectra were recorded in the range of 200–400 nm. In the reference cell, a DNA blank was placed so as to eliminate any absorbance due to DNA at the measured wavelength.

2.5.2. Competitive binding experiments

The competitive binding experiments were carried out on a Pharmacia 4000 UV–Vis spectrophotometer using 1 cm quartz microcuvettes. Absorption titrations were carried out by keeping the concentration of ethidium bromide (EB) (5.0×10^{-5} M) and DNA (5.0×10^{-5} M) constant, while varying the concentration of the complex from 0 to 5.0×10^{-5} M. The absorption spectra were recorded in the range of 300–600 nm.

2.5.3. Fluorescence spectra measurements

Fluorescence spectra were recorded on a Hitachi F-4500 fluorimeter with the emission spectral range of 550–650 nm and the slit widths of 10×5. A solution containing DNA (1.0×10^{-5} M) and EB (8.0×10^{-6} M) was titrated with varying concentrations of the complex. To the mixed DNA-EB system, the complex was steadily

added. The fluorescence intensities were measured with the excitation wavelength set at 525 nm (λ_{max} for EB) and the fluorescence emission at 592 nm (λ_{max}) was recorded.

2.5.4. Circular dichroism (CD) spectra measurements

The CD spectra were measured on a Chirascan CD spectropolarimeter at room temperature using a 0.1 cm quartz cuvette through increasing [complex]/[DNA] ratio (r = 0.0, 0.2, 0.4, 0.6, 0.8, 1.0) by steadily titrating the complex into the DNA (1.0×10^{-4} M) in 5 mM Tris–HCl/50 mM NaCl buffer solution at pH 7.2. Each sample solution was scanned in the range of 200–320 nm, and its CD spectrum was generated after averaging three scans and subtracting the buffer background.

2.5.5. Viscosity measurements

Viscosity was measured using an Ostwald Viscometer at 29 ± 0.1 °C by keeping the concentration of DNA constant (2.0×10^{-4} M), and varying the concentration of the complex from 0 to 5.0×10^{-5} M, then the flow times were measured with a digital timer. Each sample was measured three times for accuracy, and an average flow time was determined. The results were presented as $(\eta/\eta_0)^{1/3}$ versus [complex]/[DNA], where η and η_0 are the viscosity of CT-DNA solution in the presence and absence of the complex, respectively. Viscosity values were calculated according to the relation $\eta = (t - t_0)/t_0$, where t was the flow time of CT-DNA solution in the presence or absence of complex and t_0 that of the buffer alone.

2.6. DNA cleavage experiments

Electrophoresis experiments were performed using pBR322 DNA according to the established procedures. The cleavage of pBR322 DNA (250 ng) was accomplished by the addition of the Cu(II) complex in the absence and presence of 0.5 mM ascorbic acid, dissolved in 5 mM Tris–HCl/50 mM NaCl buffer at pH 7.2. The mixtures were incubated at 37 °C for 2 h. The reactions were quenched and the resulting solutions were loaded onto 0.8% agarose gels containing goldview (5 μL) for electrophoresis (120 V for 40 min in standard Tris–boric acid-EDTA buffer, pH 8). Control experiments were carried out using 20 μM $Cu(ClO_4)_2 \cdot 6H_2O$ and 20 μM ligands in the presence of 0.5 mM ascorbic acid. Goldview-stained agarose gels were imaged on a BIO-RAD Laboratories-Segrate gel imaging system, and densitometric analysis of the visualized bands was used to determine the extent of supercoiled DNA cleavage. The cleavage mechanism experiments were also carried out in the presence of typical reactive oxygen species (ROS) scavengers such as hydroxyl radical scavengers [dimethyl sulfoxide (DMSO), *tert*-butyl alcohol, and ethanol], a singlet oxygen quencher [sodium azide (NaN_3)] and a superoxide anion radical scavenger [superoxide dismutase (SOD)]. The reaction conditions used were the Cu(II) complex (15 μM) and pBR322 DNA (250 ng). Each sample was incubated at 37 °C for 2 h and analyzed according to the procedure described above.

2.7. HSA-binding experiments

2.7.1. Fluorescence measurements

Fluorescence measurements were carried out by fluorimetric titration, and on a Hitachi RF-4500 fluorescence spectrophotometer in a 1 cm path-length quartz cell. A 3.0 mL portion of aqueous solution of HSA (1.0×10^{-5} M) was titrated by successive additions of the complex (to give a final concentration of 2.6×10^{-5} M). For every addition, the mixture solution was shaken and allowed to stand for 10 min at the corresponding temperature (300 K and 310 K), and then the fluorescence intensities were measured with the excitation and emission wavelength set at 280 nm and 300–500 nm, respectively. In the meantime, the synchronous fluorescence intensity of the mixture solution was measured at $\Delta\lambda$ = 60 nm and $\Delta\lambda$ = 15 nm, respectively. For fluorescence enhancement experiments, the Cu(II) complex (5.0×10^{-6} M) in 0.05 M Tris–HCl/0.15 M NaCl buffer of pH 7.4 was titrated with HSA (to give a final concentration of 1.2×10^{-5} M). The fluorescence emission spectrum was recorded in the wavelength range of 310–600 nm with an excitation wavelength of 300 nm. Three-dimensional fluorescence spectra of HSA (1.0×10^{-5} M) in the absence and presence of the complex (1.0×10^{-5} M) were recorded in Tris–HCl buffer (pH 7.4) at room temperature.

2.7.2. Circular dichroism (CD) spectra measurements

The CD spectra of HSA were measured on a Chirascan CD spectropolarimeter at room temperature using a 0.1 cm quartz cuvette. The spectra of HSA (1.5×10^{-6} M) in the presence and absence of the complex were recorded in the range of 200–260 nm and the contents of different secondary structures of HSA were calculated from the spectral data.

2.8. Cytotoxicity assays (MTT)

Human tumor cell lines HepG2 (human hepatocellular carcinoma cells), HeLa (human cervical cancer cells) and A549 (human pulmonary carcinoma cells) were maintained in a humidified atmosphere containing 5% CO_2 at 37 °C in RPMI 1640 medium supplemented with 10% fetal bovine serum (FBS), 100 units mL^{-1} penicillin and 100 μg mL^{-1} streptomycin. A cell suspension (100 μL) were seeded into a 96-well microtiter plates at a density of 10^4 cells per well) for 24 h at 37 °C under 5% CO_2, and each well was treated with the complex in 10 μL FBS free culture medium and the plates were incubated in a 5% CO_2 humidified atmosphere for 48 h. The concentration range of the tested complex was chosen ranging from 0 to 200 μM to bracket the expected IC_{50} values. Then each well was loaded with 0.1 mg of MTT (3-(4, 5-dimethylthiazol-2-yl)-2,5-diphenyltetrazolium bromide) in 20 μL PBS (pH 7.4) for 4 h at 37 °C. The formed formazan crystals were then dissolved in 100 μL DMSO and the absorbance was measured at 570 nm using an Tecan Infinite F200 plate reader (Switzerland) [35]. Experiments were carried out in triplicate, and the percentage of cell viability was calculated using the equation, cell viability (%) = [A_{570} (sample)/A_{570} (control)] × 100%, where A_{570} (sample) refers to the reading from the wells treated with the complex and A_{570} (control) represents that treated with medium containing 10% FBS only. The IC_{50} value was determined by plotting the percentage viability versus concentration on a logarithmic graph, and the final IC_{50} value was determined by the average of four duplicate experimental results.

3. Results and discussion

3.1. Synthesis and characterization

The ligand pbt was prepared as shown in Scheme 1, and the Cu(II) complex was isolated by the reaction of glycylglycine with copper perchlorate hydrate in 80% (v/v) ethanol–water solution, with pbt as a secondary ligand (Scheme 2). The elemental analytical data is in good agreement with the molecular formula of the complex. The complex is stable in atmospheric conditions and soluble in methanol, ethanol, DMF and DMSO. The molar conductance value (89.5 Ω^{-1} cm^2 mol^{-1}) in methanol at 23 °C suggests its 1:1 electrolyte nature [36]. The ESI-MS for the complex in methanol shows a peak at m/z = 408.0 matching exactly with the coordination cation ([Cu(glygly)(pbt)]$^+$).

The IR spectrum of the complex shows a band near 3423 cm^{-1}, which is most likely ascribed to the stretching vibration ν(O—H) of the water molecule. The two broad bands near 3103 and

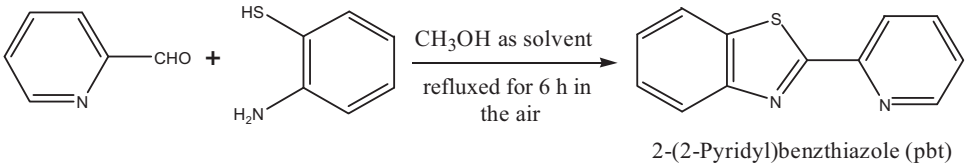

Scheme 1. Synthesis of the ligand 2-(2′-Pyridyl)benzthiazole (pbt).

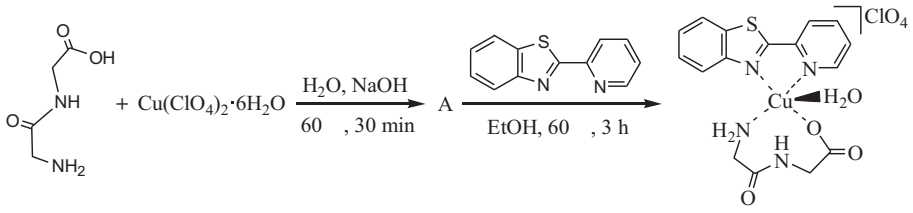

Scheme 2. Synthetic route for $[Cu(glygly)(pbt)(H_2O)]ClO_4$.

2928 cm^{-1} can be attributed to asymmetric $\nu_{as}(-NH_2)$ and symmetric stretching $\nu_s(-NH_2)$ vibrations of the coordinated and uncoordinated $-NH_2$ groups. The absence of any band in the range of 1700–1750 cm^{-1} for the complex suggests coordination of the COO^- group of the glygly to the central copper ion. The asymmetric $\nu_{as}(-COO^-)$ and symmetric stretching $\nu_s(-COO^-)$ vibrations of the coordinated carboxylate groups are 1625 and 1383 cm^{-1}. The difference value 242 cm^{-1} between $\nu_{as}(-COO^-)$ and $\nu_s(-COO^-)$ stretching frequencies is greater than 200 cm^{-1}, indicating that the carboxylate groups are coordinated to the copper ion as a monodentate group [37]. Additionally, The band at 1493 and 1561 cm^{-1} can be assigned to the ring stretching frequencies [ν(C=C) and ν(C=N), respectively] of ligand pbt, and the very strong band at 1087 cm^{-1} to ν(Cl–O) of perchlorate anions. The new non-ligand peaks at 473 and 627 cm^{-1} can be attributed to ν(Cu–O) and ν(Cu–N) stretching vibrations, respectively.

In the electronic spectra of the Cu(II) complex, three absorption bands with varied intensities were observed in methanol solution. The intense bands at 225 and 307 nm were assigned to the intraligand ($\pi \rightarrow \pi^*$) transitions of ligand pbt. Besides, much weaker and less well defined broad band observed at 638 nm in the spectra matches well with the reported $^2B_1g \rightarrow {}^2B_2g$–$(\nu_1)(d_{x2-y2} \rightarrow d_{yz})$ transition of the five-coordinated Cu^{II} in an approximate square-pyramidal geometry [38].

The thermal decomposition stoichiometry of the analytically characterized complex was determined by thermogravimetric analyses (TGA). The result showed no mass loss in the temperature range of 30–150 °C. However, in the range of 150–220 °C, a mass loss of 3.3% (calc. 3.4%; 18 mass units) was observed. This is due to the loss of one coordinated H_2O molecule from the Cu(II) complex.

Based on the above results and relevant literatures, a structure was confirmed for the complex with an approximate square-pyramidal geometry where four equatorial positions are occupied by glygly (N, O) and pbt (N, N), and the axial position is occupied by a water molecule. This coincides exactly with the reported complexes $[Cu(trp\text{-}phe)(phen)(H_2O)]ClO_4$ and $[Cu(trp\text{-}phe)(bpy)(H_2O)]ClO_4$ in a square-pyramidal geometry [38].

3.2. DNA-binding studies

3.2.1. UV spectroscopy

Monitoring the changes in the absorption spectra of metal complexes upon addition of increasing amounts of DNA is one of the most universally employed methods to determine the binding modes and binding extent of metal complexes with DNA. The

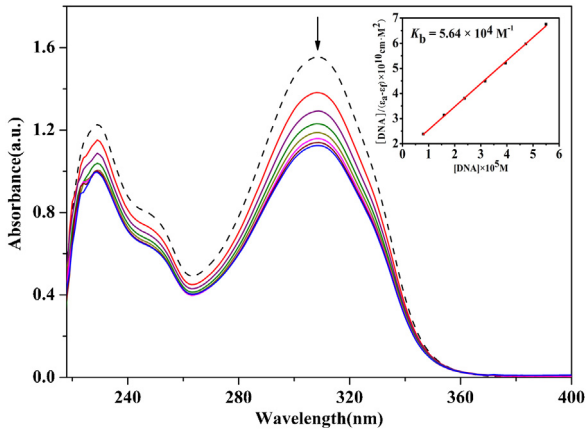

Fig. 1. Absorption spectra of the Cu(II) complex in the absence (– – –) and presence (—) of increasing amounts of CT-DNA. [Cu(II) complex] = 5.0×10^{-5} M. The arrow (↓) shows the absorbance changes upon increasing the DNA concentration. Inset: linear plot for the calculation of the intrinsic DNA binding constant (K_b).

absorption intensity of complexes may decrease (hypochromism) or increase (hyperchromism) with a slight increase in absorption wavelength (bathochromism) upon addition of DNA. In general, it is assumed that hypochromism and bathochromism are associated with the intercalative mode of metal complexes to the DNA helix involving a strong stacking interaction between aromatic chromophore and the base pair of DNA. The absorption spectra of the Cu(II) complex in the absence and presence of CT-DNA are illustrated in Fig. 1.

On addition of increasing amounts of CT-DNA to the complex, the hypochromism of the LMCT absorption band at 307 nm, along with a slight bathochromism was observed, indicating the binding of the complex to DNA by the insertion of aromatic heterocyclic ligand pbt between adjacent base pairs on the DNA duplex. The extent of the hypochromism is commonly consistent with the strength of the intercalative binding. In order to assess the DNA binding strengths of the complex, the intrinsic binding constant (K_b) for the association of the complex with CT-DNA was determined from the spectroscopic titration data using the following equation [39]:

$$\frac{[DNA]}{(\varepsilon_a - \varepsilon_f)} = \frac{[DNA]}{(\varepsilon_b - \varepsilon_f)} + \frac{1}{K_b(\varepsilon_b - \varepsilon_f)} \quad (1)$$

The 'apparent' extinction coefficient (ε_a) was obtained by calculating $A_{obsd}/[Cu]$. The terms ε_f and ε_b correspond to the extinction

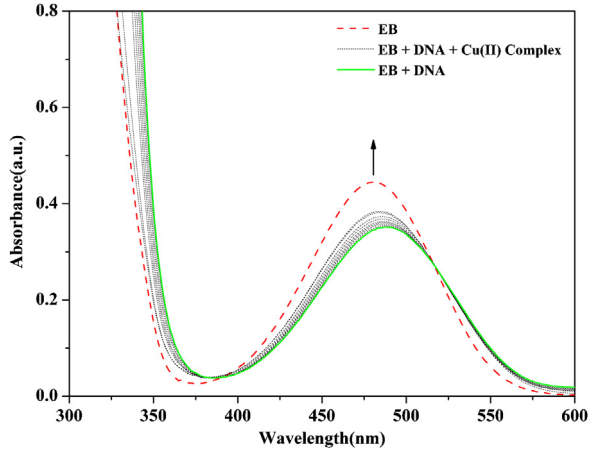

Fig. 2. Absorption spectra of free EB and EB bound to CT-DNA in the absence and presence of increasing amount of the Cu(II) complex. [EB] = [DNA] = 5.0×10^{-5} M, [Cu(II) complex] = 0.0–5.0×10^{-5} M. The arrow (↑) shows the absorbance changes upon increasing the complex concentration.

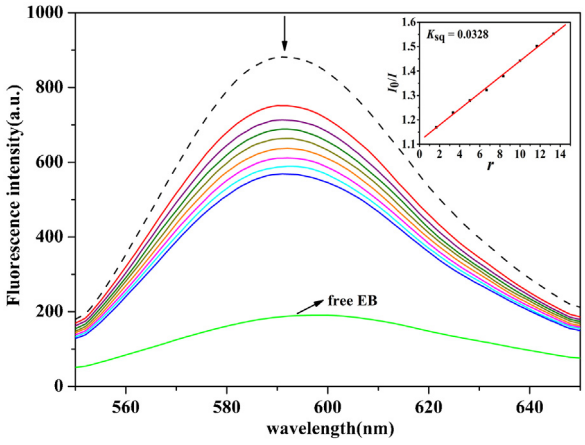

Fig. 3. Emission spectra of EB bound to CT-DNA in the absence (– – –) and presence (—) of the Cu(II) complex. [Cu(II) complex]/[DNA] = 0, 1.67, 3.33, 5.00, 6.67, 8.33, 10.00, 11.67, 13.33; λ_{ex} = 525 nm. Inset: Stern–Volmer quenching curve.

coefficients of free (unbound) and the fully bound complexes, respectively. A plot of [DNA]/($\varepsilon_a - \varepsilon_f$) versus [DNA] will give a slope of 1/($\varepsilon_b - \varepsilon_f$) and an intercept of 1/$K_b$($\varepsilon_b - \varepsilon_f$) (inset of the Fig. 1). K_b is the ratio of the slope to the intercept found to be 5.64×10^4 M^{-1}. The K_b value suggests that a modest DNA intercalative binding affinity for the complex.

3.2.2. Competitive binding assay

To further verify an intercalative binding of the Cu(II) complex to DNA, competitive binding experiment involving the addition of the complex to DNA pretreated with EB, a typical indicator of intercalation, and subsequent measurement of the absorption intensity was performed by UV–vis spectroscopy. As shown in Fig. 2, the maximum absorption peak of EB at 481 nm decreased and shifted to 488 nm after addition of DNA, which is characteristic of intercalation of EB into the DNA base pairs. Upon addition of the complex at increasing concentration to the EB-DNA system, a continuous increase in the maximum absorption and blue shift toward its original position were observed, indicating that there exists a competitive intercalation between the complex and EB with DNA, thus, releasing some free EB from the DNA–EB system [40].

3.2.3. Fluorescence quenching spectroscopy

EB is a classical intercalator that gives significant fluorescence emission intensity when it intercalates into the base pairs of DNA. When it is replaced or excluded from the internal hydrophobic circumstance of the DNA double helix by other small molecules, its fluorescence emission is effectively quenched by external polar solvent molecules such as H_2O [41]. The fluorescence quenching curves of EB bound to DNA in the absence and presence of the complex are shown in Fig. 3. A remarkable reduction in emission intensity was observed as the complex was added to the EB-DNA system, indicating that some EB molecules were replaced by the complex and released into solution from EB-DNA adduct, characteristic for the intercalative binding of the complex to DNA. The fluorescence quenching results are in good agreement with the obtained results by UV spectroscopic studies.

The quenching efficiency for each complex was evaluated by the Stern–Volmer constant K_{sq}, which varies with the experimental conditions [42]:

$$\frac{I_0}{I} = 1 + K_{sq} r \quad (2)$$

where I_0 and I are the fluorescence intensities in the absence and presence of complex, respectively, and r is the ratio of total

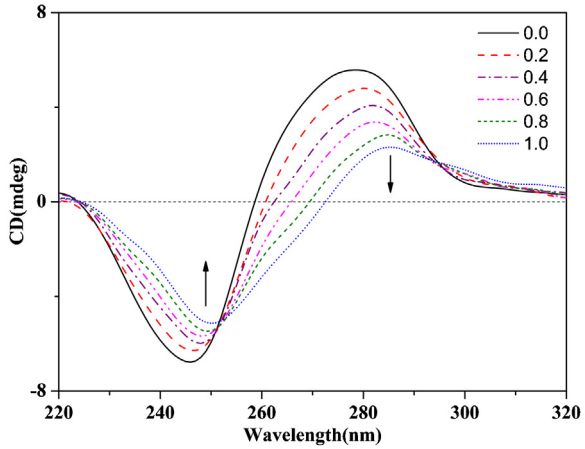

Fig. 4. CD spectra of CT DNA in the absence and presence of the Cu(II) complex in 5 mM Tris–HCl/50 mM NaCl buffer at 25 °C. [DNA] = 1.0×10^{-4} M, [Cu(II) complex]/[DNA] = 0.0, 0.2, 0.4, 0.6, 0.8, 1.0.

concentration of complex to that of DNA. K_{sq} is a linear Stern–Volmer quenching constant. The quenching plots illustrate that the fluorescence quenching of the EB-DNA system by the complex is in good agreement with the linear Stern–Volmer equation, with the K_{sq} value obtained as the ratio of the slope to intercept 0.0328 (inset of the Fig. 3).

3.2.4. CD spectroscopy

CD spectroscopy is a useful technique in diagnosing changes in DNA morphology during drug-DNA interactions. The CD spectrum of CT-DNA exhibits a positive band at 276 nm due to base stacking and a negative band at 246 nm due to the right-handed helicity of the B-DNA form, which are quite sensitive to the modes of interaction between small molecules and DNA. Simple electrostatic or groove binding interaction of complexes with DNA shows less or no perturbation of the base stacking and helicity bands, while an intercalative interaction enhances the intensities of both bands [43]. The interaction of the Cu(II) complex with DNA induced a change in the CD spectrum of B-DNA (Fig. 4). The intensities of both the negative and positive bands decreased significantly (shifting to zero levels) with the increasing concentration of the complex, accompanied with a red shift (246 → 250 nm and 276 → 285 nm for negative and positive bands, respectively), suggesting that the complex intercalated to the DNA double helix and disturbed the base stacking involving a stacking interaction between the aromatic heterocyclic

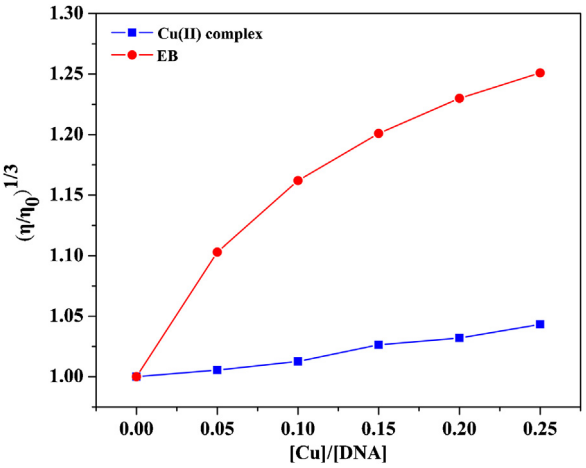

Fig. 5. Effect of increasing amounts of EB (●) and the Cu(II) complex (■) on the relative viscosities of CT-DNA at 29 ± 0.01 °C in Tris–HCl buffer. [DNA] = 2.0 × 10^{-4} M, [EB or Cu(II) complex]/[DNA] = 0, 0.05, 0.10, 0.15, 0.20, 0.25.

plane of the Cu(II) complex and the adjacent base pairs of DNA. This binding interaction induced certain conformational changes within DNA, such as the conversion from a more B-like to a more C-like structure [44]. Furthermore, the formation of the hydrogen bonds between the Cu(II) complex and DNA bases also makes some difference.

3.2.5. Viscosity determination

Optical or photo-physical properties are necessary but not sufficient to determine the binding mode of metal complexes to DNA. Viscosity is sensitive to length change and is regarded as the least ambiguous and the most critical test of a binding model in the absence of crystallographic structural data [45]. Hence viscosity measurements were employed to further verify the mode of interaction of metal complexes with DNA. A classical intercalation model demands that the DNA helix must lengthen as base pairs are separated to accommodate the binding ligand/complex, leading to an increase of DNA viscosity. In contrast, a partial intercalation of the ligand/complex could bend (or kink) the DNA helix, reduce its effective length and concomitantly its viscosity. The effect of the Cu(II) complex on the viscosity of DNA at 29 ± 0.1 °C is given in Fig. 5. The viscosity of the DNA increases steadily with the concentration of the complex, coincided with EB, a typical indicator of intercalation, which clearly emphasizes that the complex bond to DNA through an intercalative mode.

3.3. DNA cleavage studies

Agarose gel electrophoresis is a universally utilized method to investigate the chemical nucleases activity of small molecule compounds. In general, when plasmid DNA is subjected to electrophoresis, the fastest migration will be observed for the supercoiled form (Form I). If scission occurs on one strand, the supercoil will relax to generate a slower-moving nicked circular form (Form II). If both strands are cleaved, a linear form (Form III) that migrates between Form I and Form II will be obtained [46]. The observed results of the cleavage properties and mechanistic investigation are given in Figs. 6 and 7, respectively.

3.3.1. DNA cleavage in the absence and presence of ascorbic acid

As shown in Fig. 6, the Cu(II) complex in the absence of ascorbic acid does not significantly cleave the plasmid DNA (lane 6), whereas the complex shows concentration dependent relaxation of SC DNA to the NC form in the presence of ascorbic acid (0.5 mM). Under the

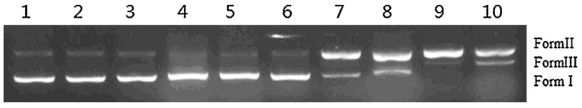

Fig. 6. Agarose gel electrophoresis patterns for the cleavage of pBR322 supercoiled DNA by the Cu(II) complex at 37 °C after 2 h of incubation. Lane 1, DNA control; lane 2, DNA + ascorbic acid (0.5 mM); lane 3, DNA + ascorbic acid (0.5 mM) + $Cu(ClO_4)_2{\cdot}6H_2O$ (20 μM); lane 4, DNA + ascorbic acid (0.5 mM) + pbt (20 μM); lane 5, DNA + ascorbic acid (0.5 mM) + glygly (20 μM); lane 6, DNA + Cu(II) complex (20 μM); lanes 7–10, DNA + ascorbic acid (0.5 mM) + Cu(II) complex (5, 10, 15 and 20 μM, respectively).

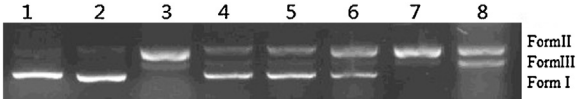

Fig. 7. Agarose gel electrophoresis patterns for the cleavage of pBR322 supercoiled DNA by the Cu(II) complex in the presence of different typical reactive oxygen species(ROS) scavengers at 37 °C after 2 h of incubation. Lane 1, DNA control; lane 2, DNA + ascorbic acid (0.5 mM) + SOD (15 units); lane 3, DNA + ascorbic acid (0.5 mM) + Cu(II) complex (15 μM); lanes 4–8, DNA + ascorbic acid (0.5 mM) + Cu(II) complex (15 μM) + [DMSO (0.2 M), *tert*-butyl alcohol (0.2 M), ethanol (0.2 M), NaN_3 (0.2 M) and SOD (15 units), respectively].

concentration of 5 μM and 10 μM, 64% and 70% of the conversion of SC DNA to NC form was achieved by the complex, respectively (lanes 7–8, respectively). With the concentration increasing to 15 μM, the Form I almost vanished, and the Form III came into sight (lane 9). When the concentration of the complex was 20 μM, the Form I disappeared absolutely, and the Form III increased significantly (lane 10). The above results demonstrate that the complex exhibits good nuclease activity in the presence of ascorbic acid.

To ensure that the Cu(II) complex was solely responsible for the cleavage, control experiments were performed (lanes 2–5, respectively) under identical experimental conditions. Free $Cu(ClO_4)_2{\cdot}6H_2O$, glygly and pbt hardly show any DNA cleavage activity in the presence of ascorbic acid (0.5 mM), even after incubation for 2 h at a considerable concentration of 20 μM, suggesting that the complex was responsible for the DNA cleavage and not the individual constituents, viz. free copper or the free ligands.

3.3.2. Mechanistic investigation of the DNA cleavage

Copper complexes can cleave DNA by hydrolytic or oxidative pathway. For an oxidative process, the complexes have been proved to react with molecular oxygen or hydrogen peroxide to generate various active oxidative intermediates (reactive oxygen species or non-diffusible copper-oxene species) [47]. In order to diagnose among the reactive oxygen species (ROS) which was responsible for the DNA cleavage catalyzed by the complex, the quenching of DNA cleavage was monitored in the presence of typical scavengers such as hydroxyl radical scavengers (DMSO, *tert*-butyl alcohol, and ethanol), a singlet oxygen quencher (NaN_3) and a superoxide scavenger (SOD) under our experimental conditions. As seen in Fig. 7, the DNA cleavage induced by the Cu(II) complex was diminished in the presence of DMSO (lane 4), *tert*-butyl alcohol (lane 5) and ethanol (lanes 6), which demonstrates that the hydroxyl radical participates in the oxidative DNA cleavage, with an inhibitory activity order observed from the extent of quenching as DMSO > *tert*-butyl alcohol > ethanol. Sodium azide had no significant effect on the DNA cleavage (lane 7). This fact rules out the involvement of $^1O_2$ or singlet oxygen-like entities [48]. On the other hand, DNA cleavage was promoted in the presence of SOD (lane 8). Futhermore, for the sake of eliminateing the influence of SOD on the DNA cleavage, control experiments of free SOD (15 units) were conducted (lane 2), which indicates that the superoxide radical anion ($O_2^{-\bullet}$) was not directly involved in the DNA strand scission but involved in a round-about way. Studies have shown that dipeptide

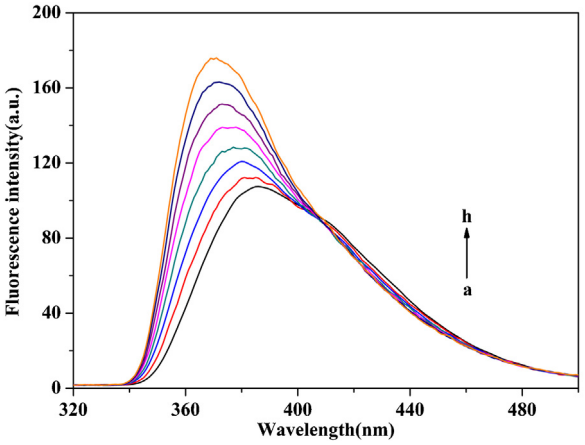

Fig. 8. Fluorescence emission spectra of the Cu(II) complex with HSA. [Cu(II) complex] = 5.0×10^{-6} M, and [HSA]/[Cu(II) complex] = 0.0, 0.2, 0.4, 0.8, 1.0, 1.2, 1.4; pH 7.4 and λ_{ex} 320 nm.

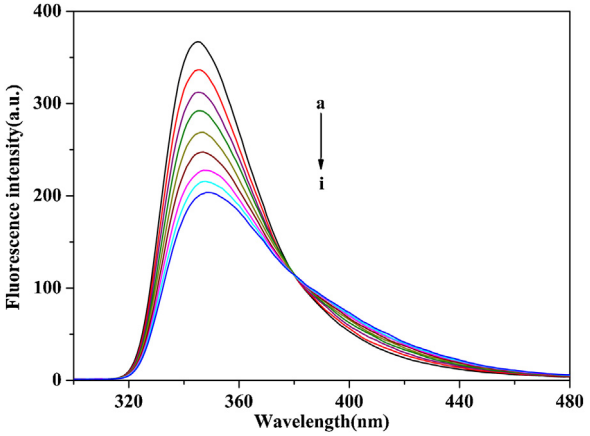

Fig. 9. Changes in the fluorescence spectra of HSA (1.0×10^{-5} M) through their titration with the Cu(II) complex. [Cu(II) complex] = 0.0–2.6×10^{-5} M; pH 7.4 and λ_{ex} 280 nm.

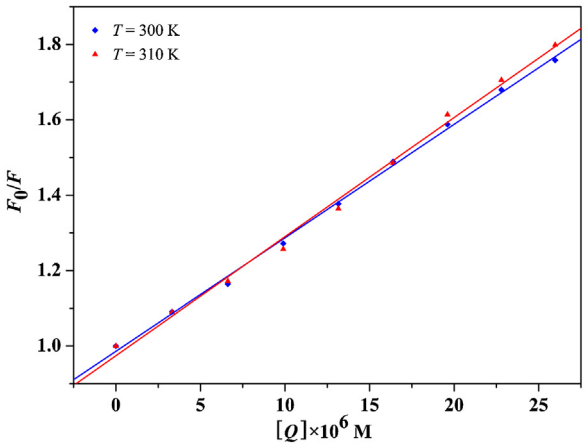

Fig. 10. Stern–Volmer plots for quenching of HSA fluorescence by the Cu(II) complex at different concentrations and temperatures (pH 7.40, λ_{ex} = 280 nm).

copper(II) complexes possess a good superoxide dismutase (SOD) activity, which can catalyze the $O_2^{-\bullet}$ to generate H_2O_2 and O_2 [43].

Based on the above results, we can safely conclude that Cu(I) species, hydroxyl radical HO• and superoxide $O_2^{-\bullet}$ are the active species involved in the DNA strand cleavage, and the following mechanistic pathway can be proposed (see Scheme 3).

3.4. HSA-binding studies

3.4.1. Effect of HSA on the fluorescence emission of the Cu(II) complex

The fluorescence titrations of the Cu(II) complex with HSA were carried out in Tris–HCl buffer of pH 7.4. As shown in Fig. 8, an increase in the concentration of HSA brings about a marked enhancement of the fluorescence intensity of the complex, coupled with a obvious blue-shifts (from 386 to 371 nm) in the fluorescence maximum, which can be attributed to the binding of the complex with the HSA resulting in a less polar microenvironment around the complex [34]. The binding of the complex to the binding pocket of HSA cut down the freedom of the complex to rotate or vibrate. This increase in rigidity can be regarded as another reason for increased emission intensity of the complex [49].

3.4.2. Fluorescence quenching studies

Fluorescence spectroscopy is an effective method used to explore the interaction between small molecules and biomacromolecules. The fluorescence emission spectra of HSA recorded in the range of 300–500 nm by exciting the HSA at 280 nm at various concentration of the Cu(II) complex are shown in Fig. 9. The HSA shows a strong fluorescence emission with a peak at 344 nm, while the complex has no intrinsic fluorescence under the present experiment conditions. The fluorescence intensities of the HSA decreased continually with increasing concentration of the complex, accompanied with a red shift (from 344 to 350 nm), indicating that the binding of the complex to HSA changed the local microenvironment around the Trp-214 residue in HSA, and concomitantly the tertiary structure of the HSA.

Commonly, fluorescence quenching can be described by the following Stern–Volmer equation [50].

$$\frac{F_0}{F} = 1 + K_{SV}[Q] = 1 + k_q \tau_0 [Q] \quad (3)$$

where F_0 and F are the steady-state fluorescence intensities in the absence and presence of quencher, respectively, K_{SV} is the Stern–Volmer quenching constant, [Q] is the total concentration of quencher, k_q is the bimolecular quenching rate constant, and τ_0 is the average lifetime of protein in the absence of quencher, and its value is 10^{-8} s. The corresponding Stern–Volmer quenching constants (K_{SV}) obtained from Fig. 10 and quenching rate constants (k_q) are given in Table 1.

The dynamic and static quenchings can be distinguished by the difference in their dependence on temperature. In the case of dynamic quenching, higher temperature results in faster diffusion and therefore the quenching rate constant increases with increasing temperature. In the case of static quenching, on the contrary, rising temperature may well bring about reducing the stability of complex and thus lower the static quenching constant [51]. Table 1 shows that the calculated K_{SV} increase with the increase of temperature, manifesting that the fluorescence quenching of HSA by the complex is likely to occur via a dynamic quenching mechanism. However, the values of k_q are much higher than the maximum value (2.0×10^{10} M^{-1} s^{-1}) for diffusion controlled quenching. This observation demonstrates that there is a specific interaction between the complex and HSA, and the probable quenching mechanism was not initiated by a dynamic process but by a static one.

3.4.3. Electronic absorption spectra studies

UV–vis absorption spectroscopy technique can be used to explore the structural changes in HSA and investigate protein–ligand complex formation. Fig. 11 shows the absorption spectra of HSA before and after the addition of the Cu(II) complex. The strong absorption peak at 208 nm originates from the

Step 1: [Cu(Ⅱ) complex] + SC DNA ⟶ [Cu(Ⅱ) complex]-----SC DNA

Step 2: [Cu(Ⅱ) complex]-----SC DNA + Vit C ⟶ [Cu(Ⅰ) complex]----SC DNA

Step 3: [Cu(Ⅰ) complex]----SC DNA + O_2 ⟶ [Cu(Ⅱ) complex]-----SC DNA + $O_2^{-\cdot}$

Step 4: [Cu(Ⅰ) complex]----SC DNA + $O_2^{-\cdot}$ + H^+ ⟶ H_2O_2 + [Cu(Ⅱ) complex]-----SC DNA

[Cu(Ⅱ) complex]-----SC DNA + $O_2^{-\cdot}$ + H^+ ⟶ O_2 + [Cu(Ⅰ) complex]----SC DNA

Step 5: [Cu(Ⅰ) complex]----SC DNA + H_2O_2 ⟶ HO· ⟶ NC DNA

Scheme 3. Possible reaction pathway for DNA cleavage.

Table 1
Quenching parameters and binding parameters of the interaction of the Cu(II) complex with HSA at different temperatures.[a]

Protein	T (K)	k_q ($\times 10^{12}$ M^{-1} s^{-1})	K_{sv} ($\times 10^4$ M^{-1})	R	K_a ($\times 10^5$ M^{-1})	n	R
HSA	300	3.175	3.175	0.998	0.708	1.069	0.998
	310	3.245	3.245	0.995	0.794	1.090	0.998

[a] R is the linear correlated coefficient.

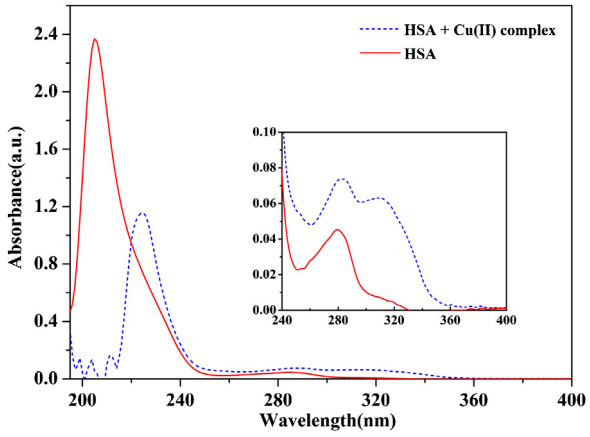

Fig. 11. UV–vis absorption spectra of HSA before and after addition of the Cu(II) complex, [HSA] = [Cu(II) complex] = 1.0 × 10^{-5} M.

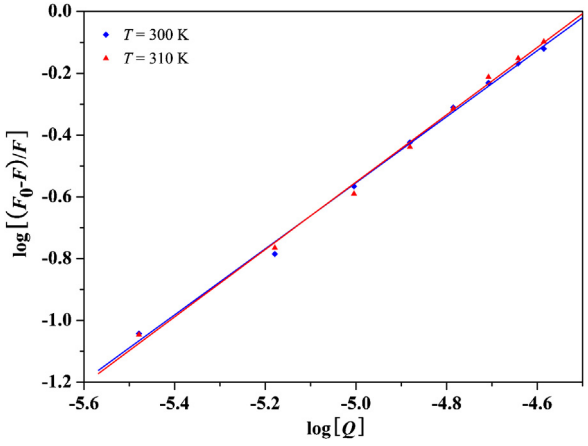

Fig. 12. Logarithmic plot of the fluorescence quenching of HSA at different temperatures.

$n \rightarrow \pi^*$ transition for the peptide bond of α-helix in HSA; the weak absorption peak at 280 nm arises from the phenyl rings in aromatic acid residues (Trp, Tyr and Phe) [52]. Upon addition of the complex, a dramatic decrease in the 208 nm absorbance peak was observed which can be put down to the induced perturbation of α-helix of HSA by a specific interaction with the complex. Besides, an obvious red shift (from 208 to 226 nm) in the position of the absorbance peak indicated that the microenvironment of Trp-214 residue in HSA was altered and the tertiary structure of the HSA was destroyed. Simultaneously, the intensity of the absorption peak at 280 nm is increased by addition of the complex, suggesting that aromatic acid residues originally buried in a hydrophobic cavity in HSA were exposed to an aqueous milieu to a certain degree. Moreover, the π–π stacking interaction between aromatic rings of the complex and phenyl rings of aromatic acid residues also made some difference. These results verified that the intrinsic fluorescence of the HSA was initiated by the complex formation between the complex and HSA rather than by the dynamic collision.

3.4.4. Binding parameters

For the static quenching, when small molecules bind independently to a set of equivalent sites on a macromolecule, the binding constant (K_a) and the numbers of binding sites (n) can be determined by the following equation [53]:

$$\log\left[\frac{(F_0 - F)}{F}\right] = \log K_a + n \log[Q] \quad (4)$$

where K_a is the binding constant, reflecting the extent of interaction between the Cu(II) complex and HSA, and n is the number of binding sites. The binding constants K_a and binding sites "n" were calculated by the intercepts and slopes, respectively, of the linear fitting plots of $\log((F_0 - F)/F)$ versus log[Q] as shown in Fig. 12 and the results have been summarized in Table 1. The binding constants increased with increasing temperature, coincided with the Lineweaver–Burk Stern–Volmer quenching constants. The value of n is nearly 1, suggesting that the complex bond to HSA according to the molar ratio of 1:1.

3.4.5. Thermodynamic parameters and binding mode studies

Ordinarily, small molecules bind to biomacromolecules through four binding modes, namely hydrogen bonding, van der Waals, electrostatic and hydrophobic interactions. The thermodynamic parameters, enthalpy change (ΔH), entropy change (ΔS) and free energy change (ΔG) are the main evidence to determine the binding mode. From the thermodynamic standpoint, $\Delta H > 0$ and $\Delta S > 0$ suggests a hydrophobic interaction; $\Delta H < 0$ and $\Delta S < 0$ indicates

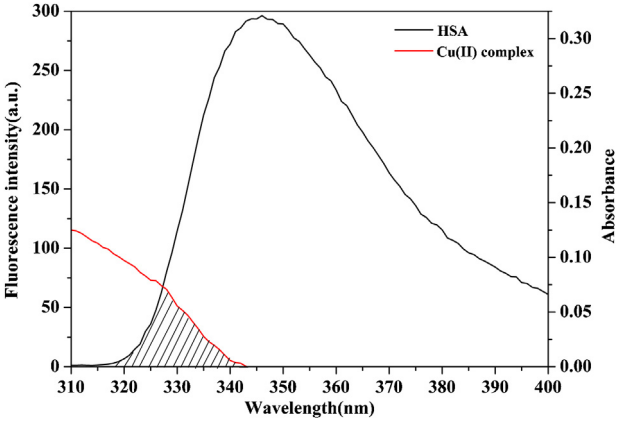

Fig. 13. Overlap of the fluorescence spectra of HSA and the absorbance spectra of the Cu(II) complex, [HSA] = [Cu(II) complex] = 1.0×10^{-5} M, T = 300 K.

the van der Waals force or hydrogen bond formation; and $\Delta H \approx 0$ and $\Delta S > 0$ reflects an electrostatic force [54]. 300 K and 310 K were chosen for the thermodynamic measurements, and the thermodynamic parameters can be calculated from the following equations:

$$\ln \frac{K_2}{K_1} = -\frac{\Delta H}{R}\left(\frac{1}{T_2} - \frac{1}{T_1}\right) \quad (5)$$

$$\Delta G = \Delta H - T\Delta S = -RT \ln K \quad (6)$$

where K is the equilibrium binding constant, which is analogous to the effective quenching constants K_a at the corresponding temperature, K_1 and K_2 are the binding constants at temperatures T_1 and T_2, respectively, and R is the gas constant. The calculated thermodynamic parameters are given in Table 2. According to the calculated data, the negative value of ΔG reveals that the complex–HSA interaction process was spontaneous. The both positive ΔH and ΔS values indicate that the hydrophobic interaction played major roles in the complex–HSA binding process and contributed to the stability of the complex.

In order to examine the electrostatic interaction between the complex and HSA, fluorescence titration was carried out by increasing the ionic strength of the HSA–complex systems through adding amounts of NaCl. The observed results suggest that the fluorescence intensity of HSA–complex was almost not changed, which makes clear that there is no electrostatic interaction in the bonding process (the data not shown).

3.4.6. Energy transfer and binding distance between the Cu(II) complex and HSA

Fluorescence energy transfer occurs via overlapping of the spectrum of a fluorophore (donor) with the absorption spectrum of a molecule (acceptor). The overlap of the absorption spectrum of the Cu(II) complex with the fluorescence emission spectrum of HSA is shown in Fig. 13. Here the donor and acceptor were HSA and the complex, respectively.

A Forster resonance energy transfer (FRET) mechanism is involved in the quenching of Trp fluorescence by complexes, the efficiency of energy transfer (E) can be given by [55]:

$$E = 1 - \frac{F}{F_0} = \frac{R_0^6}{R_0^6 + r^6} \quad (7)$$

where F and F_0 are the fluorescence intensities of HSA in the presence and absence of quencher, respectively, r is the distance between acceptor and donor, and R_0 is the critical distance when the transfer efficiency is 50%. The value of R_0 can be calculated using the equation:

$$R_0^6 = 8.78 \times 10^{-25} K^2 n^{-4} \varphi J \quad (8)$$

where K^2 is the spatial orientation factor between the emission dipole of the donor and the absorption dipole of the acceptor, n is the refractive index of the medium, φ is the fluorescence quantum yield of the donor, and J is the overlap integral of the fluorescence emission spectrum of the donor and the absorption spectrum of the acceptor and can be given by:

$$J = \frac{\int_0^\infty F(\lambda)\varepsilon(\lambda)\lambda^4 \, d\lambda}{\int_0^\infty F(\lambda) \, d\lambda} \quad (9)$$

where $F(\lambda)$ is the corrected fluorescence intensity of the donor at wavelength λ, and $\varepsilon(\lambda)$ is the molar absorption coefficient of the acceptor at wavelength λ. Under the experimental conditions, $K^2 = 2/3$, $n = 1.36$, $\varphi = 0.15$ [52], and the values of E, J, R_0 and r were calculated according to Eqs. (7)–(9) and listed in Table 2. r is on the 2–8 nm scale and $0.5R_0 < r < 1.5R_0$, suggesting the energy transfer and a static quenching interaction between the complex and HSA has occurred [56].

3.4.7. Conformation investigations

Synchronous fluorescence spectra are typically used to provide information about the molecular environment surrounding the chromophore in proteins. When the scanning interval between excitation and emission wavelength ($\Delta\lambda$) is set at 15 nm and 60 nm, the spectrum can provide the characteristic microenvironment information of tyrosine and tryptophan residues in proteins, respectively [57]. The maximum emission wavelengths of tryptophan and tyrosine residues in proteins are related to the polarity of its surroundings, and changes of the maximum emission wavelengths can reflect changes of proteins conformation. The synchronous fluorescence spectroscopy of HSA affected by the Cu(II) complex with $\Delta\lambda$ = 60 nm and $\Delta\lambda$ = 15 nm are shown in Fig. 14. The maximum emission wavelength exhibited no notable red shift at the investigated concentration range when $\Delta\lambda$ = 60 nm, suggesting that the microenvironment around the tryptophan residue did not undergo obvious changes during the binding process. However, the increasing concentration of the complex led to a significant blue shift (from 366 to 357 nm) at the maximum emission peak when $\Delta\lambda$ = 15 nm, indicating that the conformation of HSA was altered and the polarity around the tyrosine residue decreased, whereas the hydrophobicity was increased [58]. Additionally, a dramatic rise in the fluorescence intensity at $\Delta\lambda$ = 15 nm ascribes the fact that the 2-(2′-pyridyl)benzothiazole group of the complex was located in a region of the HSA where the dielectric constant is less than that of water. Therefore, the polar environment around the tyrosine is able to prevent the collision between the complex and tyrosine, the fluorescence quantum yield was improved and the fluorescence intensity of the complex–HSA system was significantly enhanced [58,59].

CD measurement was performed in the presence of the Cu(II) complex at different concentrations to ascertain the possible influence of the complex binding on the secondary structure of HSA. As Fig. 15 shows, the CD spectra of HSA (line a) exhibit two negative bands in the ultraviolet region at 208 and 222 nm assignable to $\pi \rightarrow \pi^*$ and $n \rightarrow \pi^*$ transfers for the peptide bond, respectively, which are characteristic of α-helix structure of the protein [52]. With the increasing concentration of the complex, the CD signal of both HSA increased, indicating that the binding of the complex induces a significant conformational change in HSA (lines b and c). However, the CD spectra of HSA in the presence or absence of the complex are similar in shape, suggesting that the structure of HSA is also predominantly α-helical. Furthermore, the CDNN 2.1 program was employed to quantificationally analyze the contents of different secondary structures in HSA. The histogram shows that a decreasing tendency of α-helical content while an increasing tendency of β-sheet, β-turn, and random coil structure contents were

Table 2
Thermodynamic parameters and Forster energy transfer parameters for the interaction of the Cu(II) complex with HSA at different temperatures.

T (K)	ΔH (kJ mol^{-1})	ΔG (kJ mol^{-1})	ΔS (kJ mol^{-1} K^{-1})	E	$10^{16}J$ (M^{-1} cm^3)	R_0 (nm)	r (nm)
300	8.864	−27.854	0.122	0.21	3.31	1.43	2.78
310		−29.078	0.122				

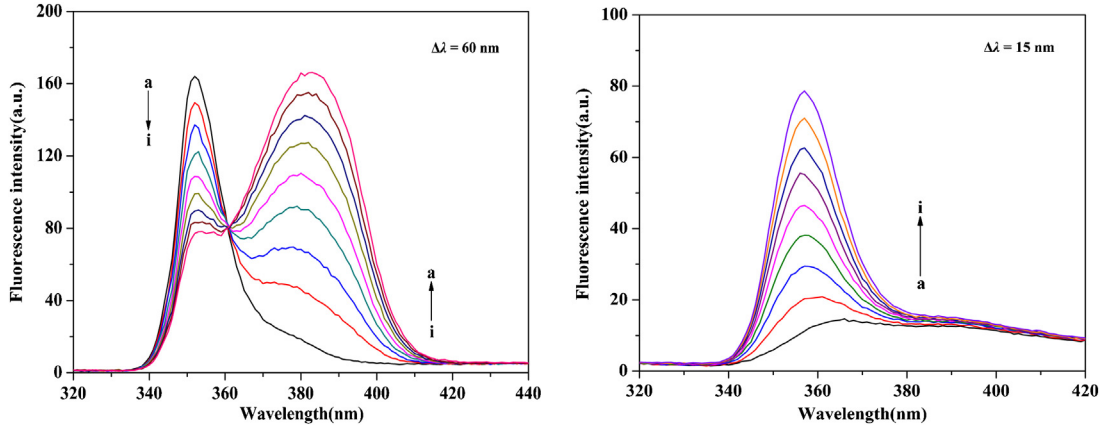

Fig. 14. Synchronous fluorescence spectra of HSA (1.0×10^{-5} M) upon addition of the Cu(II) complex at $\Delta\lambda = 60$ nm and $\Delta\lambda = 15$ nm. [Cu(II) complex] = 0.0–2.6×10^{-5} M.

observed with increasing concentration of the complex. This suggested that the complex bound with the amino acid residues of main polypeptide chain of HSA and destroyed its hydrogen bonding networks. Besides, the loss of α-helical content also indicated that the binding of the complex to HSA induced a little unfolding of the polypeptides of HSA, which resulted in the increase of the exposure of some hydrophobic regions previously buried.

To further assess the conformational changes of HSA induced by the Cu(II) complex, 3D fluorescence spectroscopy of HSA in the absence and presence of the complex were measured. By comparing the 3D fluorescence spectral changes of HSA in the absence and presence of the complex, the conformational and micro-environmental changes of HSA can be obtained. The 3D fluorescence spectra and contour ones of HSA and Cu(II) complex–HSA system are shown in Fig. 16, and the corresponding characteristic parameters are shown in Table 3. Peak a was the Rayleigh scattering peak ($\lambda_{ex} = \lambda_{em}$). Peak b (280, 336 nm, λ_{ex}, λ_{em}) mainly reflected the spectral behavior of the Trp residue, and the maximum emission wavelength and fluorescence intensity of the residue associated with its microenvironment's polarity. Peak c was the second-ordered scattering peak ($\lambda_{em} = 2\lambda_{ex}$) [60]. It was observed from Fig. 16 that the fluorescence intensities of both peaks a and b decreased significantly and the maximum emission wavelength of the peaks changed, indicating that the interaction of the complex with HSA induced some conformational and micro-environmental changes in HSA, corroborated well our spectroscopic results obtained from UV–vis, synchronous fluorescence and CD measurements.

3.5. In vitro cytotoxicity

The MTT assay was carried out to test the ability of the complex to inhibit cell growth and induce cell death in HepG2, HeLa, and A549 cancer cells. As shown in Fig. 17, the average cell viability ratio decreased with the increase of the tested complex concentration. The complex exhibit significant cytotoxic activity toward HepG2 cell lines with IC_{50} values of 17.78 μM, while considerably less active against HeLa and A549 than HepG2 cell lines, which indicates that the complex shows highly selective cytotoxicity toward HepG2 cell lines. Notably, cytotoxic effect against HepG2 for the complex (IC_{50} = 17.78 μM) is comparable to cisplatin (IC_{50} = 18.32 μM), indicating that the complex has the potential to act as an effec-

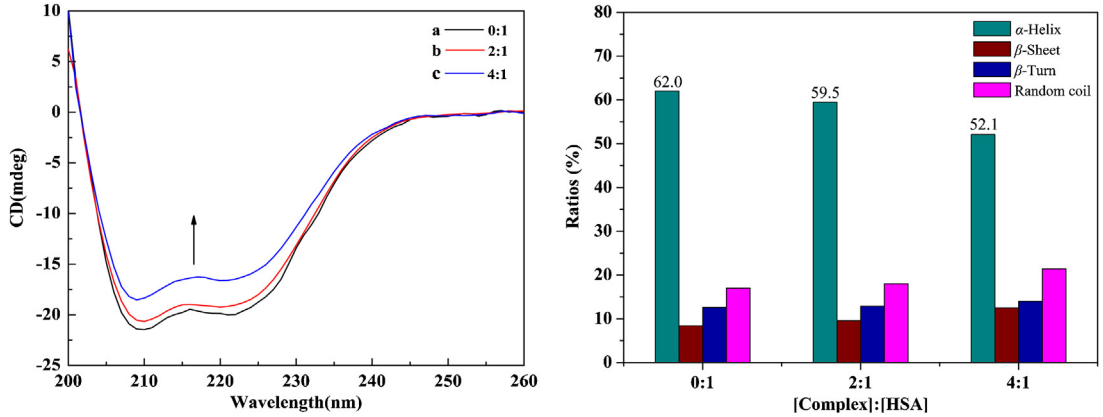

Fig. 15. CD spectra and corresponding histogram of ratio of different secondary structures of HSA in the absence and presence of the Cu(II) complex: (a) 1.5×10^{-6} M HSA; (b) 1.5×10^{-6} M HSA + 3.0×10^{-6} M Cu(II) complex; (c) 1.5×10^{-6} M HSA + 6.0×10^{-6} M Cu(II) complex. pH 7.4, at room temperature.

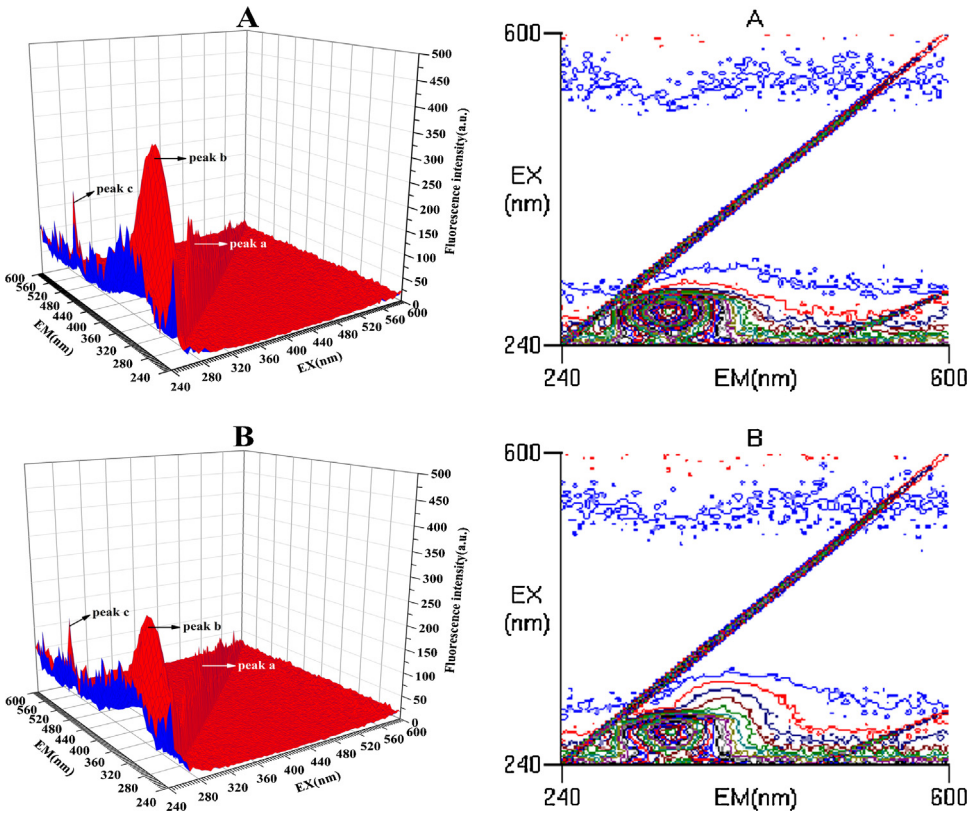

Fig. 16. 3D fluorescence spectrum and corresponding contour diagrams of HSA (A), and Cu(II) complex–HSA conjugate system (B). [HSA] = [Cu(II) complex] = 1.0×10^{-5} M. pH 7.4, at room temperature.

Table 3
3D fluorescence spectral characteristic parameters of HSA in the absence and presence of the Cu(II) complex.

HSA				HSA–Cu(II) complex system			
Peak position	$\lambda_{ex}/\lambda_{em}$ (nm/nm)	$\Delta\lambda$	Intensity	Peak position	$\lambda_{ex}/\lambda_{em}$ (nm/nm)	$\Delta\lambda$	Intensity
Peak a	280/280–360/360	0	24.26–134	Peak a	280/280–360/360	0	25.95–143.6
Peak b	280/336	56	358.9	Peak b	280/340	60	256.3

tive metal-based anticancer drugs specifically targeting HepG2. The complex shows excellent cytotoxicity against HepG2, though the affinity for DNA is not high. This could be due to the fact that DNA could not be the sole target of antitumor for the complex, and there may be other new anticancer targets, such as topoisomerase, angiogenin and other growth factors closely related with the growth and proliferation of tumor cells. It will be further investigated in the coming work.

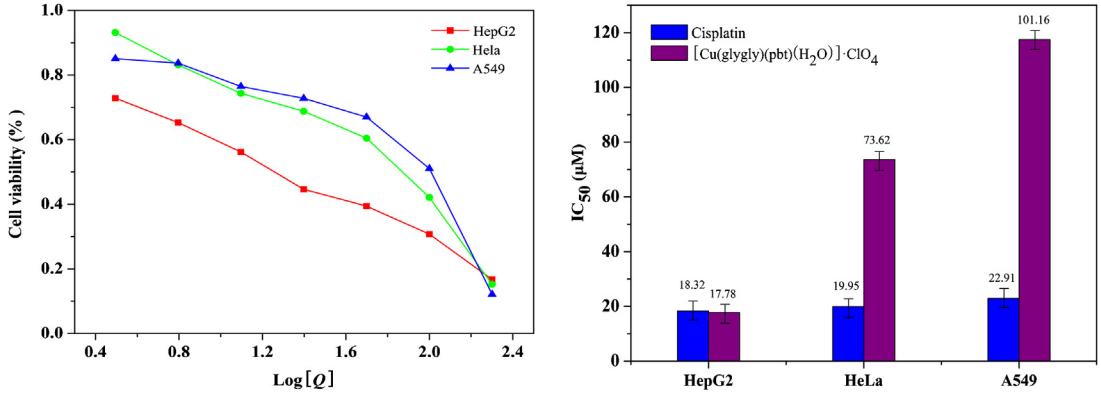

Fig. 17. The effect of the Cu(II) complex on the cells viability and the corresponding histogram of IC_{50} values for the cytotoxicity of the complex and cisplatin. [Cu(II) complex or cisplatin] = 3.125, 6.25, 12.5, 25, 50, 100, 200 μM.

4. Conclusions

In the present work, we have synthesized and characterized a new copper(II) complex derived from the dipeptide (glycyl glycine anion) and 2-(2′-pyridyl)benzothiazole. The DNA binding and cleavage, HSA interaction and anticancer activity of the complex were investigated. It was found out that the pbt based copper(II)–dipeptide complex exhibits moderate DNA-binding affinity via an intercalation mode, efficient DNA cleavage activity at a low concentration (∼5 μM) in the presence of ascorbic acid, and ideal affinity to HSA through hydrophobic interaction. Additionally, the complex possesses an excellent and selective cytotoxicity toward HepG2 cell lines (IC_{50} ∼ 17.78 μM). These findings make a clear indication that pbt based copper(II)–dipeptide complexes have the potential to be nucleic acid molecular probes and new therapeutic reagents for treating HepG2.

Acknowledgements

We are grateful to the Program of Guangdong Provincial Science & Technology (2011B020310005) and the 211 Engineering Key Project (2009B010100001) of South China Agricultural University for generous financial support.

References

[1] H. Brody, Cancer prevention, Nat. Outlook 471 (2011) S1.
[2] B. Rosenberg, L. VanCamp, J.E. Trosko, V.H. Mansour, Platinum compounds: a new class of potent antitumour agents, Nature 222 (1969) 385–386.
[3] R. Gust, W. Beck, G. Jaouen, H. Schonenberger, Optimization of cisplatin for the treatment of hormone dependent tumoral diseases. Part 1. Use of steroidal ligands, Coord. Chem. Rev. 253 (2009) 2742–2759.
[4] T. Hisano, M. Ichikawa, K. Tsumoto, M. Tasaki, Synthesis of benzoxazole, benzothiazoles and benzimidazoles and evaluation of their antifungal, insecticidal and herbicidal activities, Chem. Pharm. Bull. 30 (1982) 2996–3004.
[5] S. Bondock, W. Fadaly, M.A. Metwally, Synthesis and antimicrobial activity of some new thiazole, thiophene and pyrazole derivatives containing benzothiazole moiety, Eur. J. Med. Chem. 45 (2010) 3692–3701.
[6] N. Siddiqui, A. Rana, S.A. Khan, M.A. Bhat, S.E. Haque, Synthesis of benzothiazole semicarbazones as novel anticonvulsants – the role of hydrophobic domain, Bioorg. Med. Chem. Lett. 17 (2007) 4178–4182.
[7] R. Paramashivappa, P.P. Kumar, P.V.S. Rao, A.S. Rao, Design, synthesis and biological evaluation of benzimidazole/benzothiazole and benzoxazole derivatives as cyclooxygenase inhibitors, Bioorg. Med. Chem. Lett. 13 (2003) 657–660.
[8] H.A. Bhuva, S.G. Kinib, Synthesis, anticancer activity and docking of some substituted benzothiazoles as tyrosine kinase inhibitors, J. Mol. Graph. Mod. 29 (2010) 32–37.
[9] A. Kamal, K.S. Reddy, M.N.A. Khan, R.V.C.R.N.C. Shetti, M.J. Ramaiah, S.N.C.V.L. Pushpavalli, C. Srinivas, M. Pal-Bhadra, M. Chourasia, G.N. Sastry, A. Juvekar, S. Zingde, M. Barkume, Synthesis, DNA-binding ability and anticancer activity of benzothiazole/benzoxazole-pyrrolo[2,1-c][1,4]benzodiazepine conjugates, Bioorg. Med. Chem. 18 (2010) 4747–4761.
[10] V. Facchinetti, R.R. Reis, C.R.B. Gomes, T.R.A. Vasconcelos, Chemistry and biological activities of 1,3-benzothiazoles, Mini-Rev. Org. Chem. 9 (2012) 44–53.
[11] W.H. Liu, J.X. Chang, Y. Liu, Synthesis and antitumor activity of 5-substituted-2-(pyridyl)benzothiazole compounds, Acta Pharmaceut. Sin. 48 (2013) 83–88.
[12] E.K. Beloglazkina, I.V. Yudin, A.G. Majouga, A.A. Moiseeva, A.L. Tursina, N.V. Zyk, Synthesis and electrochemical study of 2-(2′-pyridyl)benzothiazole complexes with transition metals (Co^{II}, Ni^{II}, and Cu^{II}) Molecular structure of aquabis [2-(2′-pyridyl) benzothiazole]copper(II) diperchlorate, Russ. Chem. Bull. Int. Ed. 55 (2006) 1803–1809.
[13] P.U. Maheswari, M. van der Ster, S. Smulders, S. Barends, G.P. van Wezel, C. Massera, S. Roy, H. den Dulk, P. Gamez, J. Reedijk, Structure, cytotoxicity, and DNA-cleavage properties of the complex [Cu^{II}(pbt)Br_2], Inorg. Chem. 47 (2008) 3719–3727.
[14] K. Marjani, M. Mousavi, D.L. Hughes, Synthesis and crystal structure determination of copper(II) and iron(III) complexes of 2-(2′-pyridyl)benzothiazole, Transition Met. Chem. 34 (2009) 85–89.
[15] Y.M. Lu, Y.H. Chen, Z.B. Ou, S. Chen, C.X. Zhuang, X.Y. Le, Synthesis, antibacterial activities and nuclease properties of ternary copper(II) complex containing 2-(2′-pyridyl)benzothiazole and glycinate, Chin. J. Chem. 30 (2012) 303–310.
[16] R.N. Patel, A. Singh, K.K. Shukla, D.K. Patel, V.P. Sondhiya, Synthesis and characterization of a new nickel(II) mixed ligand complex with 2-(2′-pyridyl) benzothiazole, Indian J. Chem. A 49 (2010) 1601–1606.
[17] S.Z. Hu, D.H. Shi, T.S. Huang, J.Z. Wan, Z.X. Huang, J.L. Yang, C.H. Xu, Crystal structures and antitumor activity of 2-(2′-pyridyl)benzothiazole and its organotin complex, Inorg. Chim. Acta 173 (1990) 1–4.
[18] X.F. He, C.M. Vogels, A. Decken, S.A. Westcott, Pyridyl benzimidazole, benzoxazole, and benzothiazole platinum complexes, Polyhedron 23 (2004) 155–160.
[19] B.K. Panda, K. Ghosh, S. Chattopadhyay, A. Chakravorty, Chemistry of a new family of aryl ruthenium species incorporating alpha-diimine chelation and a pendant imine-phenol function, J. Organomet. Chem. 674 (2003) 107–115.
[20] A.A. Holder, P. Taylor, A.R. Magnusen, E.T. Moffett, K. Meyer, Y.L. Hong, S.E. Ramsdale, M. Gordon, J. Stubbs, L.A. Seymour, D. Acharya, R.T. Weber, P.F. Smith, G.C. Dismukes, P. Ji, L. Menocal, F.W. Bai, J.L. Williams, D.M. Cropek, W.L. Jarrett, Preliminary anti-cancer photodynamic therapeutic in vitro studies with mixed-metal binuclear ruthenium(II)–vanadium(IV) complexes, Dalton Trans. 42 (2013) 11881–11899.
[21] S. Tzanopoulou, I.C. Pirmettis, G. Patsis, C. Raptopoulou, A. Terzis, M. Papadopoulos, M. Pelecanou, Oxorhenium(V) and oxotechnetium(V) [NN][S]3 complexes of 2-phenylbenzothiazole derivatives, Inorg. Chem. 45 (2006) 902–909.
[22] S. Sengupta, J. Gangopadhyay, A. Chakravorty, Tertiary phosphine binding to pyridylazole chelated rhenium via substitution in phosphine oxide precursors: geometrical preference, twin isomerization and effects of diphosphine spacer length and metal oxidation state, Dalton Trans. 24 (2003) 4635–4643.
[23] J. Gangopadhyay, S. Sengupta, S. Bhattacharyya, I. Chakraboty, A. Chakravorty, Pyridylazole chelation of oxorhenium(V) and imidorhenium(V). Rates and trends of oxygen atom transfer from (ReO)–O–V to tertiary phosphines, Inorg. Chem. 41 (2002) 2616–2622.
[24] R. Czerwieniec, A. Kapturkiewicz, J. Lipkowski, J. Nowacki, Re(I)(tricarbonyl)$^+$ complexes with the 2-(2′-pyridyl)-N-methyl-benzimidazole, 2-(2′-pyridyl)benzoxazole and 2-(2′-pyridyl)benzothiazole ligands-synthesis, structures, electrochemical and spectroscopic studies, Inorg. Chim. Acta 358 (2005) 2701–2710.
[25] J.C. Mai, Z. Mi, S.H. Kim, B. Ng, P.D. Robbins, A proapoptotic peptide for the treatment of solid tumor, Cancer Res. 61 (2001) 7709–7712.
[26] S.A. Johnstone, K. Gelmon, L.D. Mayer, R.E. Hancock, M.B. Bally, In vitro characterization of the anticancer activity of membrane-active cationic peptides. I. Peptide-mediated cytotoxicity and peptide-enhanced cytotoxic activity of doxorubicin against wild-type and p-glycoprotein over-expressing tumor cell lines, Anticancer Drug Des. 15 (2000) 151–160.
[27] P.R. Reddy, P. Manjula, Mixed-ligand copper(II)-phenanthroline-dipeptide complexes: synthesis, characterization, and DNA-cleavage properties, Chem. Biodiversity 4 (2007) 468–480.
[28] C.V. Kumar, A. Buranaprapuk, Site-specific photocleavage of proteins, Angew. Chem. Int. Ed. Engl. 36 (1997) 2085–2087.
[29] F. Faridbod, M.R. Ganjali, B. Larijani, S. Riahi, A.A. Saboury, M. Hosseini, P. Norouzi, C. Pillip, Interaction study of pioglitazone with albumin by fluorescence spectroscopy and molecular docking, Spectrochim. Acta A 78 (2011) 96–101.
[30] V.T.G. Chuang, U. Kragh-Hansen, M. Otagiri, Pharmaceutical strategies utilizing recombinant human serum albumin, Pharm. Res. 19 (2002) 569–577.
[31] D.G. Churchill, Chemical structure and accidental explosion risk in the research laboratory, J. Chem. Educ. 83 (2006) 1798–1803.
[32] M.J. Waring, Complex formation between ethidium bromide and nucleic acids, J. Mol. Biol. 13 (1965) 269–282.
[33] M.F. Reichmann, C.A. Rice, C.A. Thomos, P. Doty, A further examination of the molecular weight and size of deoxypentose nucleic acid, J. Am. Chem. Soc. 76 (1954) 3047–3053.
[34] F. Samari, B. Hemmateenejad, M. Shamsipur, M. Rashidi, H. Samouei, Affinity of two novel five-coordinated anticancer Pt(II) complexes to human and bovine serum albumins: a spectroscopic approach, Inorg. Chem. 51 (2012) 3454–3464.
[35] C.Y. Gao, X. Qiao, Z.Y. Ma, Z.G. Wang, J. Lu, J.L. Tian, J.Y. Xu, S.P. Yan, Synthesis, characterization, DNA binding and cleavage, BSA interaction and anticancer activity of dinuclear zinc complexes, Dalton Trans. 41 (2012) 12220–12232.
[36] W.J. Geary, The use of conductivity measurements in organic solvents for the characterisation of coordination compound, Coord. Chem. Rev. 7 (1971) 81–122.
[37] K. Nakamoto, Infrared and Raman Spectra of Inorganic and Coordination Compounds, 4th ed., John Wiley and Sons, New York, 1986.
[38] P.R. Reddy, N. Raju, B. Satyanarayana, Synthesis, characterization, and DNA binding and cleavage properties of copper(II)-tryptophanphenylalanine-1,10-phenanthroline/2,2′-bipyridine complexes, Chem. Biodiversity 8 (2011) 131–144.
[39] A. Wolfe, G.H. Shimer Jr., T. Meehan, Polycyclic aromatic hydrocarbons physically intercalate into duplex regions of denatured DNA, Biochemistry 26 (1987) 6392–6396.
[40] B.D. Wang, Z.Y. Yang, D.D. Qin, Z.N. Chen, Synthesis, characterization, cytotoxic activity and DNA-binding properties of the Ln(III) complexes with ethylenediiminobi(6-hydroxychromone-3-carbaldehyde) schiff-base, J. Photochem. Photobiol. A 194 (2008) 49–58.
[41] C.V. Kumar, J.K. Barton, N.J. Turro, Photophysical properties of ruthenium complexes bound to double helical DNA, J. Am. Chem. Soc. 107 (1985) 5518–5523.
[42] J.R. Lakowicz, G. Weber, Quenching of fluorescence by oxygen. A probe for structural fluctuations in macromolecules, Biochemistry 12 (1973) 4161–4170.
[43] S. Tabassum, W.M. AI-Asbahy, M. Afzal, F. Arjmanda, V. Bagchi, Molecular drug design, synthesis and structure elucidation of a new specific target peptide based metallo drug for cancer chemotherapy as topoisomerase I inhibitor, Dalton Trans. 41 (2012) 4955–4964.
[44] S. Mahadevan, M. Palaniandavar, Chiral discrimination in the binding of tris(phenanthroline) ruthenium(II) to calf thymus DNA: an electrochemical study, Bioconjug. Chem. 7 (1996) 138–143.

[45] S. Satyanarayana, J.C. Dabrowiak, J.B. Chaires, Tris(phenanthroline)ruthenium(II) enantiomer interactions with DNA: mode and specificity of binding, Biochemistry 32 (1993) 2573–2584.
[46] J.K. Barton, A.T. Danishefsky, J.M. Goldberg, Tris(phenantroline)ruthenium(II): stereoselectivity in binding to DNA, J. Am. Chem. Soc. 106 (1984) 2172–2176.
[47] D.D. Li, J.L. Tian, W. Gu, X. Liu, H.H. Zeng, S.P. Yan, DNA binding, oxidative DNA cleavage, cytotoxicity, and apoptosis-inducing activity of copper(II) complexes with 1,4-tpbd(N,N,N′,N′-tetrakis(2-pyridylmethyl)benzene-1,4-diamine) ligand, J. Inorg. Biochem. 105 (2011) 894–901.
[48] F. Arjmand, M. Muddassir, R.H. Khan, Chiral preference of *l*-tryptophan derived metal-based antitumor agent of late 3d-metal ions (Co(II), Cu(II) and Zn(II)) in comparison to *d*- and *dl*-tryptophan analogues: their in vitro reactivity towards CT DNA, 5′-GMP and 5′-TMP, Eur. J. Med. Chem. 45 (2010) 3549–3557.
[49] A. Mallick, S. Chandra, S. Maiti, N. Chattopadhyay, Fluorometric investigation of interaction of 3-acetyl-4-oxo-6,7-dihydro-12H indolo-[2,3-a] quinolizine with bovine serum albumin, Biophys. Chem. 112 (2004) 9–14.
[50] L. Trynda-Lemiesz, B.K. Keppler, H. Koztowski, Studies on the interactions between human serum albumin and imidazolium (trans-tetrachlorobis (imidazol) ruthenate(III)), J. Inorg. Biochem. 73 (1999) 123–128.
[51] M.R. Eftink, C.A. Ghiron, Exposure of tryptophanyl residues in proteins. Quantitative determination by fluorescence quenching studies, Biochemistry 15 (1976) 672–680.
[52] Y.Q. Wang, X.Y. Wang, J. Wang, Y.M. Zhao, W.J. He, Z.J. Guo, Noncovalent interactions between a trinuclear monofunctional platinum complex and human serum albumin, Inorg. Chem. 50 (2011) 12661–12668.
[53] A. Divsalar, M.J. Bagheri, A.A. Saboury, H. Mansoori-Torshizi, M. Amani, Investigation on the interaction of newly designed anticancer Pd(II) complexes with different aliphatic tails and human serum albumin, J. Phys. Chem. B 113 (2009) 14035–14042.
[54] P.D. Ross, S. Subramanian, Thermodynamics of protein association reactions: forces contributing to stability, Biochemistry 20 (1981) 3096–3102.
[55] T. Forster, in: O. Sinanoglu (Ed.), Modern Quantum Chemistry, vol. 3, Academic, New York, 1996, pp. 93–137.
[56] B. Valeur, J.C. Brochon, New Trends in Fluorescence Spectroscopy, 6th ed., Springer, Berlin, 1999.
[57] N. Ibrahim, H. Ibrahim, S. Kim, J.P. Nallet, F. Nepveu, Interactions between antimalarial indolone-N-oxide derivatives and human serum albumin, Biomacromolecules 11 (2010) 3341–3351.
[58] H. Sanei, A. Asoodeh, S. Hamedakbari-Tusi, J. Chamani, Multi-spectroscopic investigations of aspirin and colchicine interactions with human hemoglobin: binary and ternary systems, J. Solution Chem. 40 (2011) 1905–1931.
[59] Y. Zheng, D.J. Chen, G.K. Wang, M.H. Xu, Y. Lu, Studies on the interaction between N-octyl-beta-*d*-glucopyranoside and bovine serum albumin, Acta Chim. Sin. 69 (2011) 633–639.
[60] Y.Z. Zhang, B. Zhou, Y.X. Liu, C.X. Zhou, X.L. Ding, Y. Liu, Fluorescence study on the interaction of bovine serum albumin with P-aminoazobenzene, J. Fluoresc. 18 (2008) 109–118.